Available online at www.sciencedirect.com
SCIENCE DIRECT®
Journal of Non-Crystalline Solids 351 (2005) 3259–3270
JOURNAL OF NON-CRYSTALLINE SOLIDS
www.elsevier.com/locate/jnoncrysol

Initiation and propagation of shear bands in Zr-based bulk metallic glass under quasi-static and dynamic shear loadings

L.F. Liu [a], L.H. Dai [a,b,*], Y.L. Bai [a], B.C. Wei [c]

[a] State Key Laboratory of Nonlinear Mechanics, Institute of Mechanics, Chinese Academy of Science, Beijing 100080, PR China
[b] State Key Laboratory of Prevention and Control of Explosion Disasters, Beijing Institute of Technology, Beijing 100081, PR China
[c] National Microgravity Laboratory, Institute of Mechanics, Chinese Academy of Science, Beijing 100080, PR China

Received 2 February 2005; received in revised form 22 July 2005
Available online 31 August 2005

Abstract

The effect of strain rate on the initiation and propagation of shear bands in the $Zr_{41.2}Ti_{13.8}Cu_{12.5}Ni_{10}Be_{22.5}$ bulk metallic glass under shear loading was investigated. The quasi-static (at a strain rate of 1.5×10^{-3} s^{-1}) and the dynamic shear tests (at a strain rate of 1.4×10^{3} s^{-1}) were conducted at room temperature using a GATAN Microtest-2000 instrument and a split Hopkinson pressure bar (SHPB) with a specially designed 'Plate-shear' specimen, respectively. The complete process of shear band initiation, propagation, and shear band unstable propagation-induced fracture was revealed. The experimental results demonstrated that the macroscopic shear strength is relatively insensitive to the strain rate, whereas shear band initiation and fracture are significantly dependent on strain rate. A dimensionless Deborah number was introduced to characterize the effect of the strain rate on the formation of shear bands. Additionally, the observed numerous liquid droplets and melted belts on the fracture surface at high-strain rates demonstrate that the adiabatic heating exerts a significant effect on fracture behavior of the material.

PACS: 71.23.C; 47.20.F; 62.20.F; 62.20

1. Introduction

Recently, bulk metallic glasses (BMGs) have attracted large interest due to their unique physical, mechanical, and chemical properties [1–6]. However, BMGs loaded under the unconstrained conditions usually fail catastrophically with little global plasticity [7,8]. This deformation behavior has limited the application of BMGs as engineering materials so far. At low temperatures (e.g. room temperature), plastic deformation of BMGs is usually localized into thin shear bands [9,10]. Many macroscopic mechanical properties (e.g. plasticity and ductility) are thus controlled by the individual and collective behaviors of the shear bands. Therefore, the initiation, propagation and fracture of localized shear bands in metallic glasses have been the subject of both theoretical and experimental investigations for number of years [11–25].

Generally speaking, a shear band is usually initiated at a local region where the viscosity or the resistance of the material to deformation is greatly reduced. There has been considerable debate in the literature as to the cause of this reduction, and two hypotheses emerged to explain why local changes in viscosity occur in shear bands. The first suggests that the reduction of viscosity within shear bands is resulted from the generation and coalescence of free volume. This idea was originated in the work of Spaepen, who developed a plastic flow model based on a

* Corresponding author. Address: State Key Laboratory of Nonlinear Mechanics, Institute of Mechanics, Chinese Academy of Science, Beijing 100080, PR China. Tel.: +8610 62616852; fax: +8610 62579511.
E-mail address: lhdai@lnm.imech.ac.cn (L.H. Dai).

0022-3093/$ - see front matter © 2005 Elsevier B.V. All rights reserved.
doi:10.1016/j.jnoncrysol.2005.07.030

competition between stress-driven creation and diffusional annihilation of free volume [11]. Subsequent works from Argon [12], Stief et al. [13], Li et al. [23], and Wright et al. [26] also supported the free volume hypothesis. The second hypothesis is that local adiabatic heating beyond the glass transition temperature, or even the melting temperature, thus leading to the deformation softening, is the main cause for formation of shear bands in BMGs. This idea was proposed by Leamy et al. [27] who attributed the vein pattern morphologies of fracture surfaces to the adiabatic heating of the deformed region. This hypothesis was supported by Liu et al. [28] who observed liquid droplets on the fracture surfaces of the tested samples. However, the precise physical nature of the formation mechanism of shear bands in BMGs still remains unclear.

On the other hand, it is noted that the generation and coalescence of free volume, thus the initiation and propagation of shear bands, are significantly affected by loading conditions and strain rates. Under compressive load, metallic glasses deform and fracture along localized shear bands and the fracture angle, θ_C, between the compressive axis and shear plane is smaller than 45° (about 42°) [29–31]. Under tensile load, however, it is found that the tensile angle, θ_T, between the tensile axis and the fracture plane is larger than 45°. In most cases, θ_T is in the range 50–65° with an average value of 56° [32–34]. Simultaneously, the deformation and fracture behavior of metallic glasses at room temperature have an obvious strain rate effects. Owen et al. [35] found that the dynamic fracture toughness of a Zr based BMG dramatically increased with increasing loading rates at room temperature. Bruck et al. [36] reported that the compressive strength of a Zr based BMG was independent of strain rates. Hufnagel et al. [37] observed that the uniaxial compression failure stress decreased with increasing strain rates. Maddin and Masumoto [38] showed that the fracture stress of $Pd_{80}Si_{20}$ filament decreased with increasing strain rates. Kawamura et al. [39] also reported that the tensile strength of a rapidly solidified $Zr_{65}Al_{10}Ni_{10}Cu_{15}$ ribbon specimen decreased with increasing strain rates. Strain rate not only affects the fracture strength but also exerts a significant influence on the formation of shear bands in BMGs. Mukai et al. [40] reported that the density of shear bands formed in a Pd-based BMG under tensile loadings increased with strain rates. This phenomenon was supported by recent nanoindentation investigations on BMGs, which were made, respectively by Schuh et al. [41–44], Nieh et al. [45], Jiang and Atzmon [46], and Dai et al. [47]. However, further works are still need to discern the effect of strain rate on formation and propagation of shear bands in BMGs.

Apparently, the strain rate dependency of deformation behavior in BMGs varies with material components, specimen shapes and loading procedures. Furthermore, most available experimental studies on shear banding in BMGs were conducted under uniaxial compression and indentation loadings. However, the complicated stress state in the testing sample makes it difficulty to elucidate clearly the physical nature of shear banding in BMGs. Different from the compression or indentation loading mode, the relative simple stress state is achieved in the sample subjected to a shear loading. To the authors' knowledge, the investigations on plastic deformation and shear banding behavior of BMGs subjected to a shear loading are very limited to date. In view of aforementioned observations, the strain rate effects on shear banding in the $Zr_{41.2}Ti_{13.8}Cu_{12.5}Ni_{10}Be_{22.5}$ bulk metallic glass under quasi-static and dynamic shear loadings were investigated. By controlling applied load and limiting deformation, the complete process of shear band initiation, propagation, and shear band unstable propagation induced fracture patterns was obtained. Also, the free volume theory based constitutive model originally developed by Spaepen [11] was modified to characterize the observed strain rate-dependent shear banding behavior of the material. Based upon this modified model, the strain rate effect on the initiation and propagation of shear bands was discussed as well in this paper.

2. Experimental procedure

2.1. Specimens preparations

The $Zr_{41.2}Ti_{13.8}Cu_{12.5}Ni_{10}Be_{22.5}$ bulk metallic glass was produced by arc melting the pure elements together under a purified Ar atmosphere in ingots of the desired composition; each ingot was then re-melted fourth to ensure a homogeneous composition. From these ingots, metallic glass plates with 100 mm in length, 20 mm in width, and 2 mm in thickness were prepared by suction casting the molten alloy into a copper mold. The obtained metallic glass plates were confirmed to be non-crystalline by conventional X-ray diffraction.

In order to conduct shear test, the specimens were specially machined into 'Plate-shear' shape, which is shown in Fig. 1. The 'Plate-shear' specimen shear technique was originally introduced by Meyer and Manwaring [48], which was used successfully for investigating adiabatic shear banding in a number of materials [49,50]. This method can force shear localization occur in a narrow region. Different from the narrow ring-shaped shear zone in Meyer's hat-shaped specimen, the shear area in our present 'Plate-shear' shaped specimen is a narrow flat zone. The observed surfaces of samples were finely polished before loading.

2.2. Mechanical tests

Quasi-static and dynamic shear tests of the $Zr_{41.2}Ti_{13.8}Cu_{12.5}Ni_{10}Be_{22.5}$ bulk metallic glass were con-

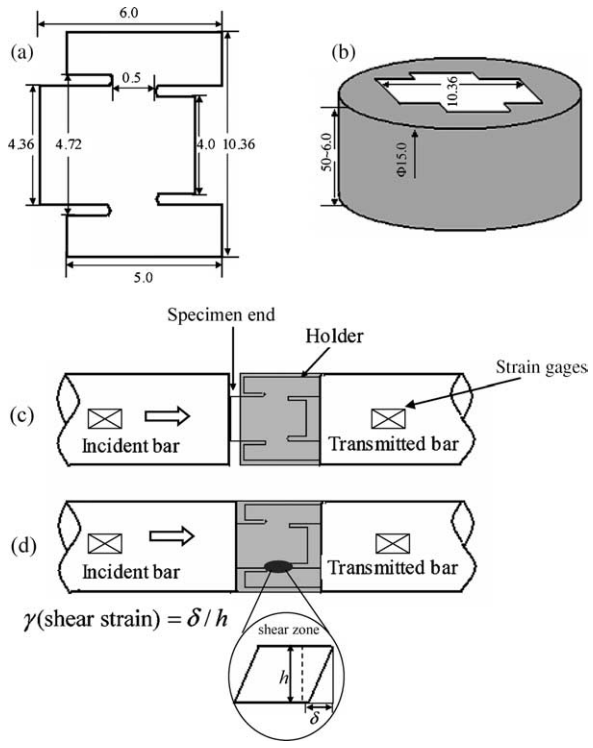

Fig. 1. Schematic diagram of shear test set-up: (a) the 'hat-like-shaped' specimen (dimensions in mm), (b) the holder, (c) before loading, (d) after loading.

ducted using a Microtest-2000 (GATAN) instrument and a split Hopkinson pressure bar (SHPB) at a room temperature, respectively. In our tests, the amount of the shear displacement is controlled by the length of the specimen end outside the steel holder, which is shown in Fig. 1(c) and (d). By adjusting this length and the applied load, different shear deformation stages can be achieved in the shear zone. As a result, the process of the initiation and propagation of shear bands in BMGs can be revealed by this technique. The average shear stresses can be calculated according to the force balance of the shear deformation unit. While the averaged shear strains can be estimated by measuring the displacement, δ, and the thickness of the shear zone h, which is shown in Fig. 1(d). In the present work, h is defined as the horizontal distance of centers of the upper and lower notches. The value of h was measured with a light microscopy (POLYVAR-MET, Reichert-Jung, Austria).

In the present work, to assure the measurements with an adequate accuracy and minimize the systematic errors, the minimum calibration of measurements of the displacement δ, the thickness h, and the force were 0.01 μm, 0.1 μm and 0.1 N, respectively. In our tests, the range of δ from the initiation to fracture of shear bands was 6.10–8.32 μm, the range of h was 380.1–420.9 μm, and the range of force was 861.4–1720.8 N. So, in our measurements, the estimated systematic errors did not exceed 0.1%. Simultaneity, to obtain reliable

Table 1
Shear stress of the initiation (A), propagation (B) of shear bands and peak shear stress (C)

Strain rate (s^{-1})	A (MPa)	B (MPa)	C (MPa)
1.5×10^{-3}	900 ± 25	990 ± 30	1100 ± 35
1.4×10^{3}	900 ± 30	990 ± 40	1100 ± 50

macroscopic stresses corresponding to the initiation, propagation, and fracture of shear bands at both strain rates, at least 12 specimens were performed for each case. The measured values with the corresponding random errors were given in Table 1. The random error was estimated by $\Delta x_{\max} = x_{\max} - x_{\min}$, where $x_{\max}$ and $x_{\min}$ stands for the measured maximum and minimum values, respectively. In the quasi-static strain rate shear experiments, the average shear strain rate, which was estimated by the velocity of the load head and the shear zone size, was fixed at $1.5 \times 10^{-3}\ s^{-1}$. In SHPB dynamic shear experiments, the specimen was embedded inside the high-strength steel holder, which as a whole was sandwiched between the incident and the transmitted bars. To acquire loading pulses, two pairs of strain gages were bonded at the mid-span of the incident and the transmitted bars. According to the obtained loading pulses and the standard SHPB principle, the average shear stress, the shear strain, and the shear strain rate can be determined. In our dynamic shear tests, the average shear strain rate was fixed at $1.4 \times 10^{3}\ s^{-1}$ by controlling impact velocity. In the dynamic testing, since the cross-area of high-strength steel holder is much larger than that of deformed region in the specimen, the deformation of specimens can be automatically interrupted by steel holder as soon as the incident bar contacts the steel holder. Fig. 2(a) and (b) are the oscillograms of the input and the output wave pulses achieved at the dynamic strain rate tests at the fixed striking velocity. It is well known that, in dynamic experiments, the amplitudes and platform of oscillograms represent the magnitudes and duration of loading pulses. Fig. 2(a) demonstrated that, at the fixed striking velocity, the shapes of the input oscillograms were almost identical, whereas the shapes of the output oscillograms, as shown in Fig. 2(b), were different. The difference between the input and output oscillograms showed that the experimental materials deformed plastically. The difference among the output oscillograms, especially before the marked loading limitation line (at this point of oscillograms, the loading pulse arrived at the specimen holder and further deformation was limited), was caused by the deformation-controlled technique. Because the amplitudes stand for the magnitudes of the loads, through the deformation-controlled technique, the applied loads on different specimens were controlled at different levels. The amplitudes of output oscillograms before the loading limitation line shown in Fig. 2(b) represent the magnitude of load.

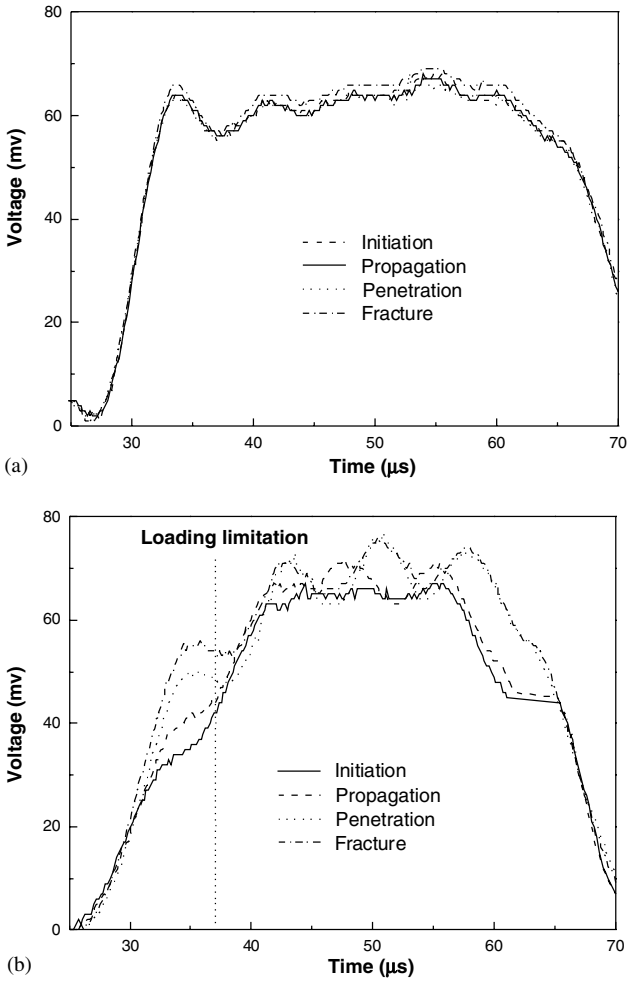

Fig. 2. The oscillograms of the input and the output waves in split Hopkinson pressure bars tests.

From Fig. 2, one can find that, the applied load on the specimen could be controlled at different magnitudes. Thus, the shear deformation can be interrupted at different stages. The results demonstrated that this deformation-controlled technique is feasible.

With this deformation-controlled technique, a series of tests were conducted at quasi-static rates and dynamic strain rates, and the average shear stress–strain curves and the shear fracture stresses (shear strength) were obtained. After testing, all the samples were examined by a scanning electron microscope (SEM, FEI-Sirion NC microscope) to reveal the character of initiation, propagation, and fracture surface morphologies of the material.

3. Experimental results

3.1. Mechanical behavior

The average shear stress–strain curves of the present bulk metallic glass $Zr_{41.2}Ti_{13.8}Cu_{12.5}Ni_{10}Be_{22.5}$ at quasi-static strain rates ($1.5\times10^{-3}\ s^{-1}$) and dynamic strain rates ($1.4\times10^{3}\ s^{-1}$) are shown in Fig. 3. It can be seen from Fig. 3 that, for both typical strain rates, the material exhibits a 'quasi-brittle' behavior and little macroscopic plastic flow (about 0.1%). After the peak stress, the stress dropped to its zero value immediately. The peak shear stress or shear strength is about 1100 ± 50 MPa for both the quasi-static and dynamic strain rates. This means that the shear strength of this alloy is relatively insensitive to the strain rate. The present result is consistent with the experimental observation of Lu–Ravichandran–Johnson in compressive mode [24]. The obtained quasi-static shear strength, 1100 ± 35 MPa, is almost identical to the experimental result made by Chen et al. [51] in torsional shear mode for the identical alloy. Additionally, the shear stresses corresponding to shear band initiation, propagation, and critical failure of the samples, which are marked as A, B, and C, respectively in Fig. 3, are displayed in Table 1. It can be seen from Table 1 that these shear stresses are also insensitive to the strain rate.

3.2. Initiation and propagation of shear bands

The initiation and propagation of shear bands at quasi-static strain rates are illustrated in Fig. 4. The experimental observations have indicated that shear bands were initiated in the tip of the notch in the specimen when the average shear stress reached about 900 ± 25 MPa. This stress point is marked as 'A' in Fig. 3. The initiated shear bands, which exhibit bright lines under SEM observations, are shown in Fig. 4(a). With the applied load increasing to point 'B' shown in Fig. 3, one shear band, which is located in the middle of shear region, propagates quickly while the others propagate little. At this deformation stage, the evolution

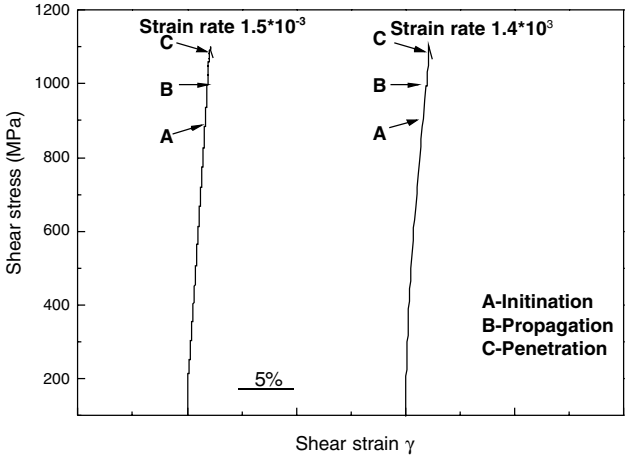

Fig. 3. Shear stress–strain curves of the $Zr_{41.2}Ti_{13.8}Cu_{12.5}Ni_{10}Be_{22.5}$ BMG at different strain rates.

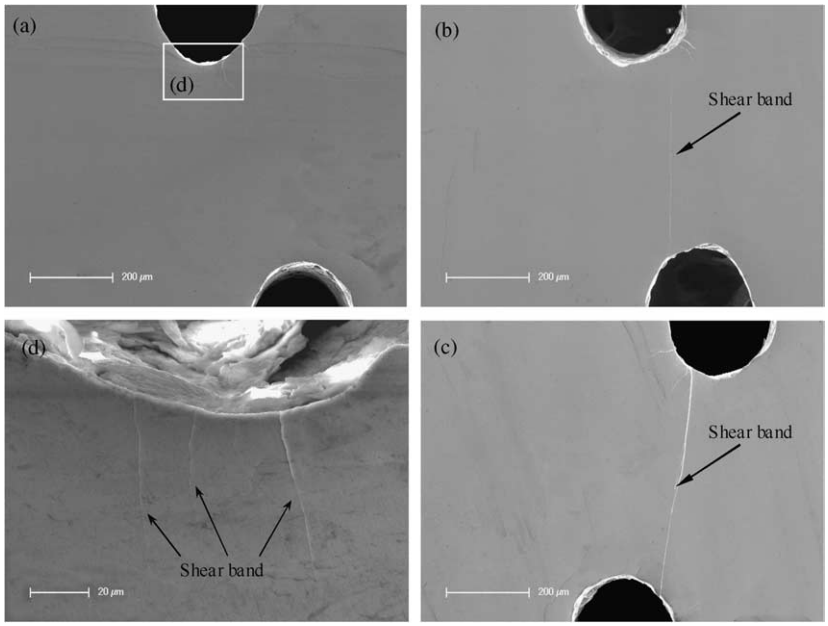

Fig. 4. The SEM micrographs of the evolution of shear bands in the $Zr_{41.2}Ti_{13.8}Cu_{12.5}Ni_{10}Be_{22.5}$ BMG under strain rates 1.5×10^{-3} s^{-1}: (a) initiation, (b) propagation, (c) penetration.

pattern of shear bands is shown in Fig. 4(b). When the load continued increasing and the peak shear stress of about 1100 ± 35 MPa was reached, which corresponds to the point 'C' in Fig. 3, the dominated shear band penetrated across the whole deformation region which is shown in Fig. 4(c) and the specimen fractured immediately along this full-developed shear band.

At dynamic strain rate, the initiation and evolution of shear bands are presented in Fig. 5(a)–(c), respectively. The corresponding stress levels are also marked, respectively as A, B, C in Fig. 3. Compared with the quasi-static strain rate case, the evolution of shear bands at dynamic strain rate is of the following features: (1) The average shear stress levels under which shear bands were initiated and penetrated across the whole shear region in the specimen are almost the same as those in the quasi-static case, i.e. 900 ± 30 MPa and 1100 ± 50 MPa, respectively. This means that the macroscopic critical shear stresses corresponding to shear band initiation and propagation are relatively insensitive to strain rates. (2) The density of shear bands initiated at dynamic strain rates is higher than that at quasi-static strain rates, which is demonstrated clearly in Figs. 4(d) and 5(d). This observation is consistent with the findings of Mukai et al. [40] in dynamic tensile mode, and Schuh et al. [41–44], Nieh et al. [45], Jiang and Atzmon [46], and Dai et al. [47] in nanoindentation mode. The difference in the density indicates that the initiation of shear bands is significantly dependent on the strain rate. The mechanism for such a strain rate-dependent shear banding behavior will be discussed in next section.

3.3. Fracture surface morphology

To understand shear band propagation and shear fracture mechanisms of the material, both quasi-static and dynamic shear fracture surfaces were carefully examined by SEM (FEI-Sirion NC microscope). The SEM micrographs of the side view of the typical fracture surfaces at these two typical strain rates are presented in Fig. 6(a) and (b), respectively. It is readily observed that, under both quasi-static and dynamic loads, samples fracture along a single shear plane, indicating one major shear band dominates the final fracture. The result demonstrates that the 'Plate-shear' shaped specimen can effectively ensure the deformation under the prescribed simple shear condition. The micrographs of the fracture morphologies at both typical strain rates are shown in Figs. 7 and 8, respectively.

3.3.1. Quasi-static fracture features

The typical fracture morphology of the $Zr_{41.2}Ti_{13.8}Cu_{12.5}Ni_{10}Be_{22.5}$ BMG under quasi-static shear loading is shown in Fig. 7(a). It can be seen from Fig. 7(a) that the fracture surface can be divided into three characteristic zones [52,53] along shear band propagation direction, which are the fracture slip zone (I), the facture propagation zone (II) and the unstable fracture zone (III) in turn. In the slip zone (I), except for some thinner ridges and valleys across the whole region, the surface along the ridges and valleys (also is the shear direction, as indicated by arrow) is relatively smooth. In the zone (II), the speed of the crack became fast and different

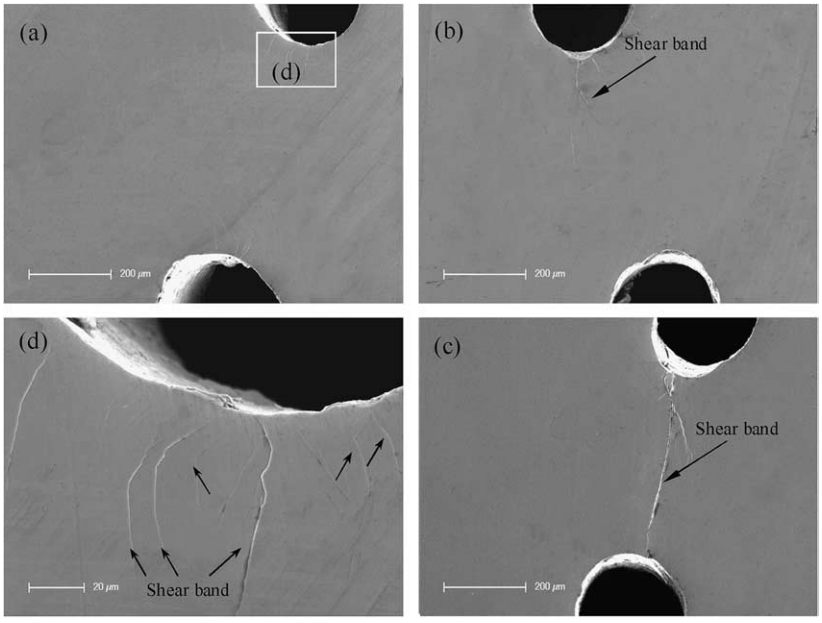

Fig. 5. The SEM micrographs of the evolution of shear bands in the $Zr_{41.2}Ti_{13.8}Cu_{12.5}Ni_{10}Be_{22.5}$ BMG under strain rates $1.4 \times 10^3\ s^{-1}$: (a) initiation, (b) propagation, (c) penetration.

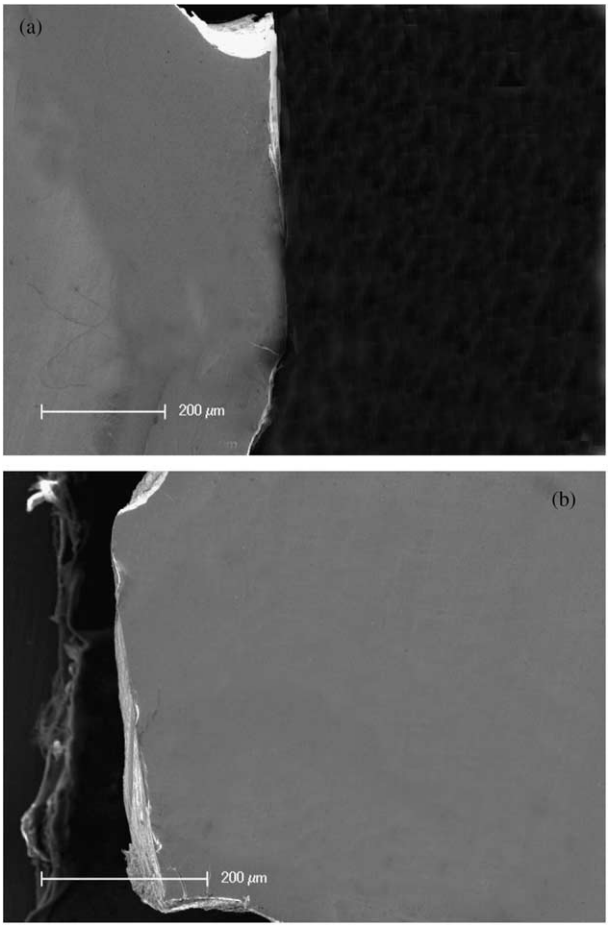

Fig. 6. A side view of the fractured sample: (a) strain rate $1.5 \times 10^{-3}\ s^{-1}$, (b) strain rate $1.4 \times 10^3\ s^{-1}$.

morphological patterns were formed along the shear band propagation direction. Firstly, numerous strips can be observed in the early stage of zone (II). It is interesting that these strips were initially thin and then became gradually thicker. With the crack propagating further, lots of striated vein patterns were formed. In this region, several micro-cracks with width of about 10 μm can be seen, which is shown in Fig. 7(b). At the late stage of the zone-II (Fig. 7(c)), the size of the micro-cracks became larger while the number was fewer than that in the middle stage of zone-II, and the striated vein patterns were transformed into cell-like vein patterns. Fig. 7(d) is a typical high-magnification micrograph of the cell-like vein patterns formed in the zone-II. Compared with the vein patterns formed in the compressive experiments [25], there is no droplet of metallic glass observed. Additionally, the tails of cells were obviously stretched. The difference in the fracture surface morphologies formed in shear mode and in compression or tension mode demonstrates that normal stress exerts an influence on the fracture behaviors of BMGs. As the crack progressed further and advanced into the zone-III, its velocity was accelerated to a critical value and the crack became unstable. The crack propagated unstably and facture led to a jagged structure on the fracture surface, as illustrated in Fig. 7(e). This jagged structure means that the fracture process in the zone-III is discontinuous. Actually, such a three-stage fracture feature can also be found in other brittle materials, such as PMMA, where the fracture surface experiences 'mirror', 'mist', and 'hackle' three stages along the direction of the crack propagation [53].

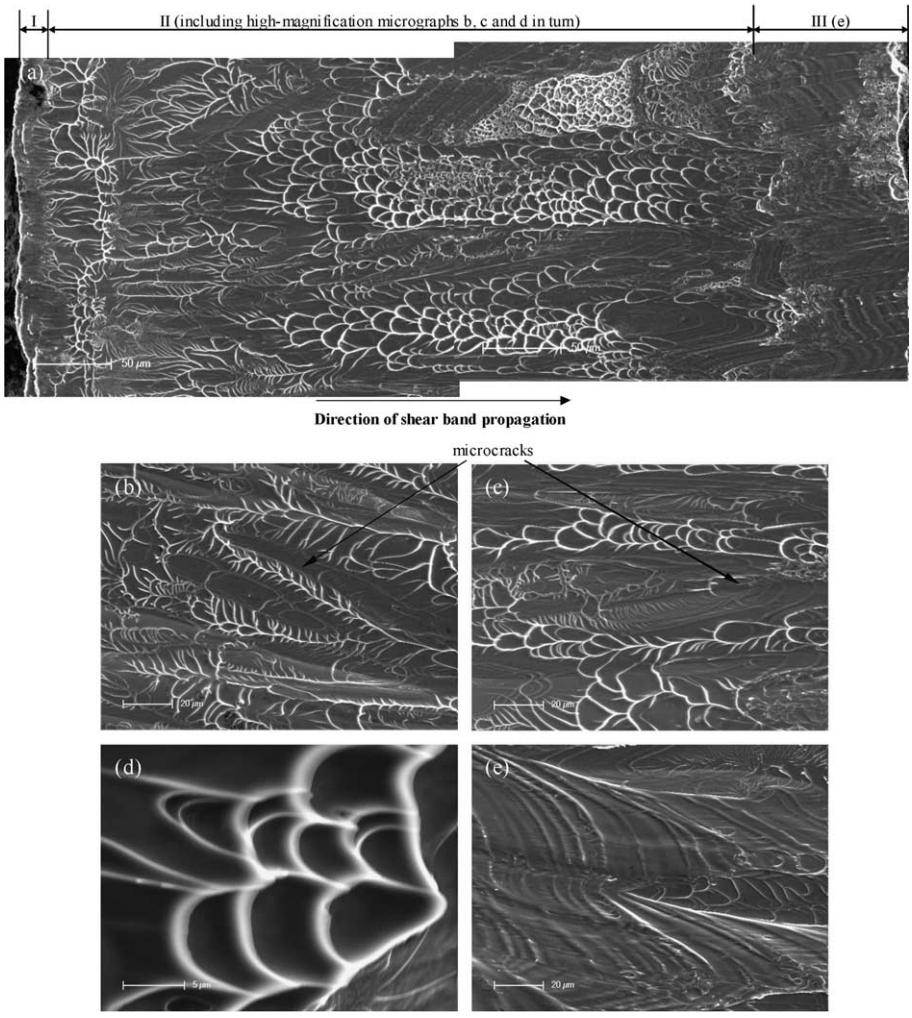

Fig. 7. The fracture morphologies under quasi-static shear load: (a) the full image of fracture processes along shear band propagation direction, (b) high magnification of striated vein patterns and micro-cracks in zone II, (c) high magnification of cell-like vein patterns and micro-cracks in zone II, (d) cell-like vein patterns in zone II, (e) a jagged structure in zone III.

3.3.2. Dynamic fracture feature

Fig. 8 is the typical fracture surface morphology of the $Zr_{41.2}Ti_{13.8}Cu_{12.5}Ni_{10}Be_{22.5}$ bulk metallic glass under dynamic shear loading. Similar to the quasi-static case, the fracture surface under dynamic shear loading can also be divided into three zones along the direction of the crack propagation, namely the fracture slip zone (I), the fracture propagation zone (II) and the unstable fracture zone (III) in turn. However, compared with the quasi-static case, several different characteristic features of the fracture morphology become evident. These features are summarized as follows: (1) the fracture surface is relatively rough in comparison with the quasi-static strain rate case. (2) In the zone-II, the array of patterns is relatively disorder. As shown in Fig. 8(b), the size of the micro-cracks is larger and the number is fewer than under quasi-static loading. Simultaneity, the micro-cracks and valleys were distributed randomly. It is noted that, many melted droplets and belts can be obviously observed in the late stage of the zone-II, as illustrated in Fig. 8(a)–(c). The melted droplets and belts indicate that the temperature rise induced by the adiabatic shear heating may exceed the melting temperature of the alloy. (3) Besides jagged structure, some cell-like vein patterns can also be observed in the zone-III, as shown in Fig. 8(e).

Figs. 7 and 8 show a full fracture propagation process of the tested Zr-based bulk metallic glass under quasi-static and dynamic strain rates, respectively. For both strain rate cases, fracture was initiated from one dominant shear band and developed along the direction of this dominant shear band. From a macroscopic view, shear fracture experiences three characteristic stages referred as facture initiation-slip, fracture propagation, and unstable fracture for both quasi-static and dynamic cases.

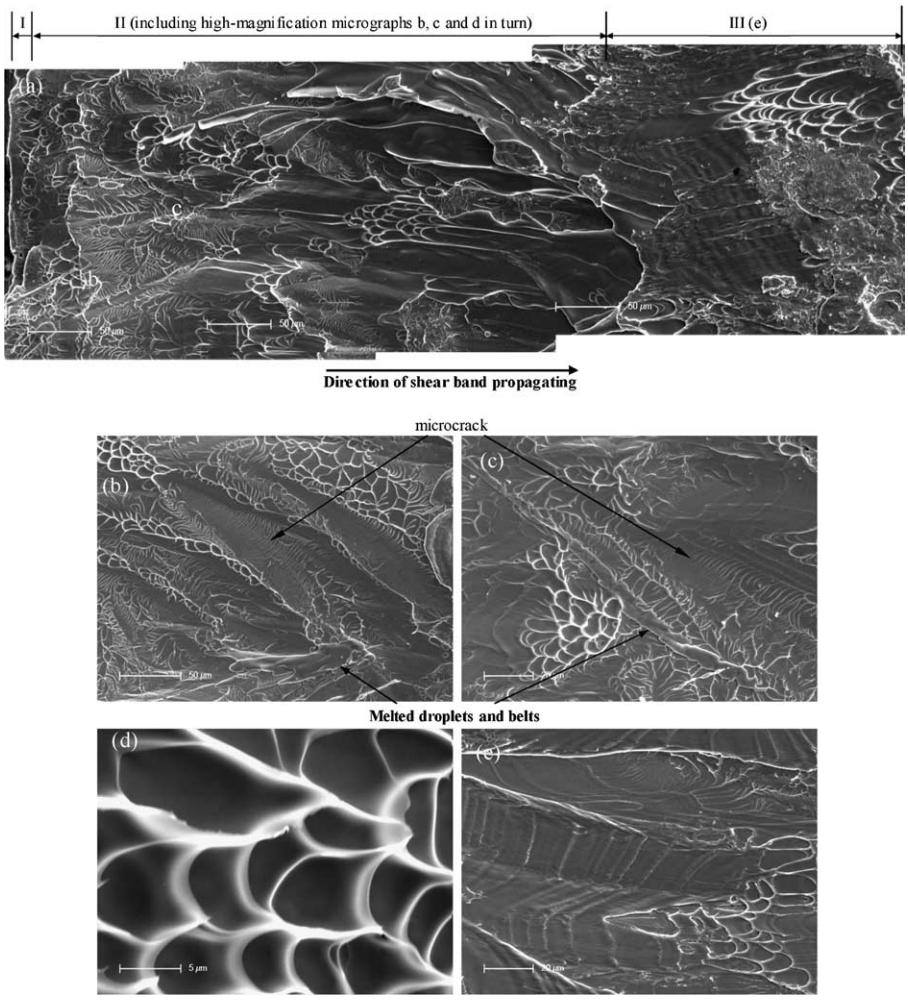

Fig. 8. The fracture morphologies under dynamic shear load: (a) the full image of fracture processes along shear direction, (b) high magnification of striated vein patterns and micro-cracks in zone II, (c) high magnification of cell-like vein patterns and micro-cracks in zone II, (d) cell-like vein patterns in zone II, (e) a jagged structure in zone III.

4. Discussion

From the above experimental results and observations, it can be seen that the initiation, propagation, and fracture morphology are affected greatly by the strain rate, although the shear strength for this alloy is relatively insensitive to the stain rate. However, the mechanisms for this rate-dependent shear banding behavior are not well understood.

As is shown in Fig. 3, the shear strength of the $Zr_{41.2}Ti_{13.8}Cu_{12.5}Ni_{10}Be_{22.5}$ metallic glass is independent of strain rates at room temperature. This observation is similar to the observation made by Lu et al. [25] in the compression mode for the identical alloy. However, the initiation of shear bands is strongly dependent on the strain rate. It can be found from Figs. 4(a) and 5(a) that the number of shear bands initiated at dynamic strain rates is larger than that at quasi-static strain rates. This result is consistent with the reports of Mukai et al. [40] on the $Pd_{40}Ni_{40}P_{20}$ BMG in tension test, Schuh and Neih [41] on $Pd_{40}Cu_{30}Ni_{10}P_{20}$, Nieh et al. [45] on $Zr_{10}Al_5Ti_{17.9}Cu_{14.6}Ni_{47.5}$, and Dai et al. [47] on the $Zr_{41.2}Ti_{13.8}Cu_{12.5}$–$Ni_{10}Be_{22.5}$ in nanoindentation test. Simultaneously, many available investigations have demonstrated that the local coalescence of the free volume is an important reason for the formation of shear bands at the early deformation stage of BMGs [10–13,21,22]. Hence, the difference in the density of initiated shear bands at quasi-static and dynamic strain rates may be due to the effect of the strain rate on the generation of free volume in BMGs.

According to the free volume theory [11–13], the formation of shear bands in metallic glasses is mainly due to the creation and coalescence of the free volume in some local regions, whereas the creation and diffusion of free volume in metallic glasses are affected greatly by the strain rate. Based on Turnbull–Cohen's free volume theory [54,55], Spaepen developed a general con-

stitutive equation to characterize plastic flow of metallic glasses [11]. According to this model, the shear strain rate can be written as

$$\dot{\gamma} = \frac{\dot{\tau}}{\mu} + 2f \cdot \exp\left(-\frac{\alpha}{\xi}\right) \cdot \exp\left(-\frac{\Delta G}{k_B T}\right) \cdot \sinh\left(\frac{\tau\Omega}{2k_B T}\right), \tag{1}$$

where τ is the applied shear stress, $\dot{\gamma}$ the shear strain rate, ξ the concentration of the free volume, α a geometrical factor of order unity, f the frequency of atomic vibration, ΔG the activation energy, Ω the atomic volume, k_B the Boltzmann's constant, μ the shear modulus and T the absolute temperature. Eq. (1) shows that the concentration of the free volume ξ plays a key role in the deformation of metallic glasses. An as-prepared metallic glass is thermodynamically unstable and has a non-equilibrium amount of free volume. During the deformation under the shear stress, the concentration of the free volume is continuously created by an applied shear stress and annihilated by structure relaxation due to atom rearrangement. In the flow model developed by Spaepen [11], the free volume is created by an applied shear stress τ and annihilated by a series of atomic jumps, and the net rate of the change of concentration of free volume is

$$\frac{\partial \xi}{\partial t} = f \cdot \exp\left(-\frac{\alpha}{\xi}\right) \cdot \exp\left(-\frac{\Delta G}{k_B T}\right) \cdot \left\{\frac{2\alpha k_B T}{S\xi V^*}\left(\cosh\left(\frac{\tau\Omega}{2k_B T}\right) - 1\right) - \frac{1}{n_D}\right\}, \tag{2}$$

where n_D is the number of atomic jumps needed to annihilate a free volume equal to V^*, and $S = \frac{2(1+\nu)}{3(1-\nu)}\mu$, ν is the Poisson's ratio. By numerically solving Eqs. (1) and (2), the shear stress–strain and evolution of the concentration of free volume can be obtained. In the calculation, we take $\alpha = 0.15$, $f = 1 \times 10^{13}\ \mathrm{s}^{-1}$, $\Delta G = 1 \times 10^{-19}$ J, $\Omega = 26.1 \times 10^{-30}\ \mathrm{m}^3$, $k_B = 13.8 \times 10^{-24}$ J/K, $\mu = 35.3$ GPa, $V^* = 0.8\ \Omega$, $\nu = 0.36$, $T = 300$ K. The shear stress and the concentration of free volume are assumed to 0 and 0.008, respectively in the initial configuration. According to calculations, the effect of strain rate on the dimensionless free volume concentration is presented in Fig. 9. It can be seen from the figure that the dimensionless free volume concentration is strongly sensitive to the shear strain rate, i.e. the dimensionless free volume concentration increases with increasing shear strain rate. The variations of the dimensionless shear stress and free volume concentration with shear strain are for a typical strain rate $\dot{\gamma} = 1.0 \times 10^{-2}\ \mathrm{s}^{-1}$ are shown in Fig. 10(a). It can be seen that, for those relatively low stresses, the free volume annihilation rate exactly balances the stress-driven creation rate. As a result, the total concentration of free volume remains constant. With the applied load increasing further, the creation rate exceeds the annihilation rate, which results in a catastrophic drop in shear stress. Eventually, the annihilation rate again balances the creation rate, and the steady state value of the concentration of free volume are reached. It is noted from Fig. 10(a) that the steady value of the concentration of free volume is larger than the initial value. More importantly, it can be found from Fig. 9

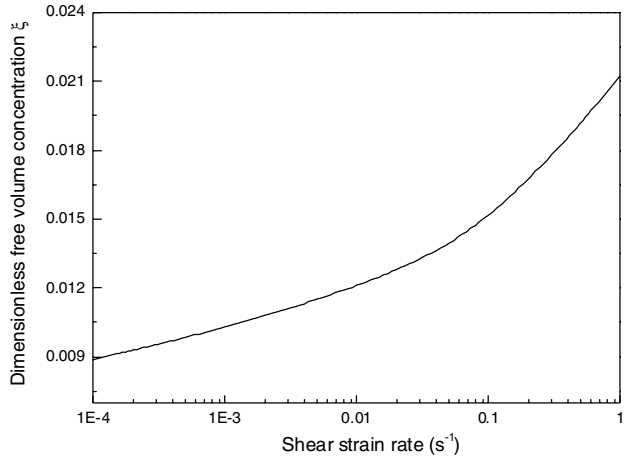

Fig. 9. Variations of dimensionless free volume concentration with shear strain rates.

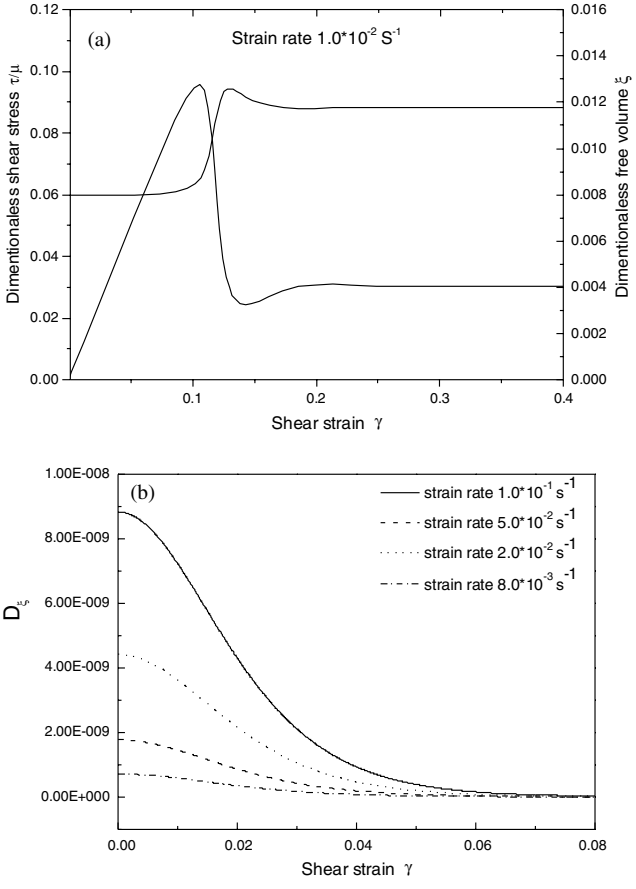

Fig. 10. The calculated results: (a) dimensionless shear stress, free volume concentration varied with shear strain, (b) Deborah varied with shear strain for different strain rates.

that the total concentration of free volume in metallic glasses is significantly affected by the strain rate, and the higher the strain rate the higher the concentration of free volume. According to free volume theory, the coalescence of free volume is a key reason for the formation of shear bands in BMGs. Therefore, the relatively higher concentration of free volume will provide a strong driving force for initiation of shear bands in BMGs.

A question naturally arises: why the free volume concentration at high-strain rate is larger than that at low-strain rate. As mentioned above, the coalescence of free volume in BMGs is controlled by the competition between the stress-driven creation process and the annihilation process due to structural relaxation. Furthermore, both the stress-driven creation and the structural relaxation processes are tightly related to the macroscopic deformation response to applied loading. So, we can introduce a dimensionless Deborah number, namely the ratio of the structural relaxation time scale to the macroscopic deformation response time to characterize the free volume coalescence in BMGs. Deborah number was initially introduced by Reiner to characterize how 'fluid' a material is [57]. Recently, Bai et al. [58] have demonstrated that this dimensionless number is a key parameter for charactering damage evolution and damage localization of materials. In the present case, we defy dimensionless Deborah number as

$$De = t_r/t_i, \tag{3}$$

where $t_r = \eta/\mu$ is the structural relaxing time of BMGs under shear load, $t_i = 1/\dot{\gamma}$ is the macroscopic imposed time of applied stress or the characteristic time of macroscopic deformation. Here, $\eta = \tau/\dot{\gamma}$ is the viscous coefficient, and $\dot{\gamma}$ is the shear strain rate defined as Eq. (1). According to Eq. (3), one can find that the larger Deborah number De is, the slower the structural relaxation annihilation process of free volume is. So, a relatively larger Deborah number De will lead to a relatively higher free volume concentration in BMGs.

Based on Eqs. (1)–(3), the variations of Deborah number with shear strain at different strain rates are shown in Fig. 10(b). From the figure, one can find that the values of Deborah number De at high-strain rates are larger than those at low-strain rates in the early deformation stage. The relatively larger De at high-strain rates demonstrates that the relative annihilation of free volume is slower than that at low-strain rates. Therefore, the concentration of the free volume at high-strain rates is higher than that at low-strain rates. The present and other experimental observations [40–47] that the number of shear bands initiated at high-strain rate is larger than that at low strain rate could be mainly attributed to this reason. The remaining question is that why the shear stress is insensitive to strain rate while the initiation of shear bands is dependent on the strain rate? As in the aforementioned analysis, the concentration of the free volume at high-strain rates is higher than that at low-strain rates. According to the free volume theory [11–13], the formation of shear bands in metallic glasses is mainly due to the creation and coalescence of the free volume in some local regions, whereas the creation and diffusion of free volume in metallic glasses are affected greatly by the strain rate. Thus, this strain rate effect of the free volume leads to that initiation of shear band depends on the strain rate in metallic glasses. However, once the shear bands were initiated, with shear deformation increasing, one of the shear bands will rapidly propagate along the deformation zone while the others propagate little. Obviously, the macroscopic shear stress (i.e. peak stress) under the present unconstraint conditions is controlled by the propagation behavior of a single main shear band. The effect of strain rate on the macroscopic stress is mainly determined by the ratio of the characteristic time of macroscopic deformation to that of propagation of shear band. In dynamic strain rate case, the characteristic time of macroscopic deformation can be estimated as $t_i = 1/\dot{\gamma} \sim 10^{-3}$ s. While the characteristic time of propagation of shear band is determined by the propagation speed of shear band and the size of the deformation zone. The magnitude order of the propagation speed of shear band in BMGs is about $\sim 10^2$ m/s and the characteristic size of the shear deformation zone is 1 mm. So, the characteristic time of propagation of shear band is about 10^{-5} s. Obviously, the strain rate-controlled characteristic time of macroscopic deformation is much larger than that of the propagation of shear bands. Therefore, the strain rate exerts little effect on the propagation of shear bands, which in turn leads to that macroscopic stress is relatively insensitive to strain rate.

However, this does not mean that the local heating induced by the dissipated deformation work does not play a role in the formation of shear bands in BMGs for any cases. At high-strain rates ($\dot{\gamma} \geqslant 10^2\ s^{-1}$), the local heating within shear localization zone may exert an influence on the shear band formation in BMGs. Hence, a further study is still needed to be performed to discern this effect at high-strain rates.

Once shear bands were initiated in the alloy, one dominant shear band will propagate fast and fracture occurs immediately. Figs. 7 and 8 show the fracture morphologies at the quasi-static and dynamic strain rates, respectively. Since fracture morphology is created by shear band propagation, a close-up examination on the characteristic features of fracture morphology can help us understand the shear band propagating behaviors and fracture mechanisms. It can be seen from Figs. 7 and 8 that the facture morphologies at quasi-static and dynamic shear loading are quite different. On the whole,

the fracture surfaces at dynamic strain rates are relatively rough in comparison with the quasi-static case. Especially, under dynamic loading, numerous liquid droplets and melted belts can be clearly observed, which are shown in zone-II in Fig. 8. However, during the early propagation stage of shear bands, i.e. zone-I and the beginning stage of zone-II, such melting phenomenon cannot be found. This means that the local temperature rise cannot exceed the melting temperature of the alloy in the formation and initial propagation stages. However, as the deformation proceeds further, numerous liquid droplets and melted belts can be found in the late stage of the zone-II. This means that the adiabatic shear induced temperature rise in shear bands exceeds the melting temperature of the tested material.

According to the observed shear-steps on the surfaces of the shear deformation regions, the average shear strain within shear bands formed at dynamic strain rate is estimated as 5.5. For high-strain rate case, the deformation can be considered approximately to be an adiabatic process. Hence, the temperature rise in the shear bands, $\Delta\theta$, can be estimated by the following equation:

$$\Delta\theta = \frac{K\tau\gamma}{\rho c_p}, \tag{4}$$

where τ and γ are the average shear stress and the shear strain in shear bands, respectively, ρ is the mass density of the alloy, c_p is the specific heat, K ($\cong$0.9) is the work-heat transformation coefficient. For the present material, $\rho = 6000\ \text{kg/m}^3$, $c_p = 450\ \text{J/(kg K)}$ [56]. According to the experimental results, $\tau = 1100\ \text{MPa}$, $\gamma = 5.5$. Inserting these values into Eq. (4), the possible temperature rise in shear bands is 2016 K. The melting temperature of the tested materials is 936 K. Obviously, the adiabatic shear induced temperature rise in shear bands during dynamic shearing exceeds the melting temperature of the material. This is why numerous liquid droplets and melted belts can be clearly observed on the fracture surfaces at dynamic strain rates. It is noted that a similar high-adiabatic temperature rise in BMGs was observed by the other investigators recently. By using high-speed infrared technique, Bruck et al. [26] detected an increased temperature >500 °C in sample surface zone of the identical alloy under dynamic compressive loading at room temperature. Liu et al. [28] reported that there was a 900 K-temperature rise inside shear bands in a Zr–Al–Cu–Ni bulk metallic glass subjected to a tensile loading. It is noted that the relatively rough fracture surface and the melted droplets in the fracture surface at dynamic strain rates means that the dissipated energy during dynamic shearing is larger than that during quasi-static case. This is perhaps the reason for the measured fracture toughness of the identical alloy being dramatically increased at high-strain rates [35].

5. Conclusions

In this paper, a systematic study on the strain rate effect on the initiation and propagation of shear bands in the $Zr_{41.2}Ti_{13.8}Cu_{12.5}Ni_{10}Be_{22.5}$ bulk metallic glass under shear loading was made. Quasi-static and dynamic shear tests at room temperature were carried out by using a Microtest-2000 (GATAN) instrument and a split Hopkinson pressure bar (SHPB) with a specially designed 'Plate-shear' shaped specimen and the deformation controlling technology. We have shown that the macroscopic shear strength and fracture strain were insensitive to the strain rate. However, the initiation of shear bands and the final fracture surface patterns were affected significantly by the strain rate. It was observed that the number of shear bands formed at high-strain rates is larger than that at low-strain rates. To understand this strain rate-dependent shear banding behaviors, the free volume theory based constitutive model developed by Spaepen [11] and a dimensionless Deborah number were introduced to characterize the effect of the strain rate on the form of shear bands. Both the experimental and numerical investigations reveal that the creation and coalescence of free volume play an important role in the formation of shear bands in bulk metallic glasses. The local heating effect on the formation of shear bands in BMGs at high-strain rates is needed to be a further study.

A close-up microscopic examination showed that the fracture surfaces can be divided into three characteristic zones: fracture slip zone, fracture propagation zone and unstable fracture zone for quasi-static and dynamic strain rate cases. However, the concrete features within these three zones at dynamic strain rates were quite different from those at quasi-static strain rates. The most striking feature of the fracture surface at dynamic strain rates is that numerous liquid droplets and melted belts can be clearly observed in the zone-II on the fracture surface. The temperature rise inside shear bands was estimated to be 2016 K. This means that adiabatic heating affects greatly the fracture behaviors of this bulk metallic glass.

Acknowledgments

The authors gratefully acknowledge the financial support of this work by the National Natural Science Foundation of China through grants 10472119 and 10232040.

References

[1] A.L. Greer, Science 267 (1995) 1947.
[2] W.L. Johnson, MRS Bull. 24 (1999) 42.

[3] A. Inoue, Acta Mater. 48 (2000) 279.
[4] J.J. Kim, Y. Choi, S. Suresh, A.S. Argon, Science 295 (2002) 654.
[5] K.F. Kelton, T.K. Croat, A.K. Gangopadhyay, L.Q. Xing, A.L. Greer, M. Weyland, X. Li, K. Rajan, J. Non-Cryst. Solids 317 (2003) 71.
[6] W.H. Wang, C. Dong, C.H. Shek, Mater. Sci. Eng. R 44 (2004) 45.
[7] H.A. Bruck, T. Christman, A.J. Rosakis, W.L. Johnson, Acta Metall. Mater. 30 (1994) 429.
[8] Xueshan Xiao, Shoushi Fang, Lei Xia, Weihuo Li, Qin Hua, Yuanda Dong, J. Non-Cryst. Solids 330 (2003) 242.
[9] C.A. Pampillo, Scr. Metall. 6 (1972) 915.
[10] R.D. Conner, W.L. Johnson, N.E. Paton, W.D. Nix, J. Appl. Phys. 94 (2003) 904.
[11] F. Spaepen, Acta Metall. 25 (1977) 407.
[12] A. Argon, Acta Metall. 27 (1979) 47.
[13] P.S. Steif, F. Spaepen, J.W. Hutchinson, Acta Metall. 30 (1982) 447.
[14] P.E. Donvan, W.M. Stobbs, Acta Metall. 29 (1981) 1419.
[15] T. Zhang, A. Inoue, Mater. Trans. JIM 39 (1998) 857.
[16] C.C. Hays, C.P. Kim, W.L. Johnson, Phys. Rev. Lett. 84 (2000) 2901.
[17] T.C. Hufnagel, P. EI-Deiry, R.P. Vinci, Scr. Mater. 43 (2000) 1071.
[18] R. Vaidyanathan, M. Dao, G. Ravichandran, S. Suresh, Acta Mater. 49 (2001) 3781.
[19] K.M. Flores, R.H. Dauskrdt, Acta Mater. 49 (2001) 2527.
[20] W.J. Wright, R. Saha, W.D. Nix, Mater. Trans. JIM 42 (2001) 644.
[21] J.S. Langer, Phys. Rev. E 64 (2001) 01154.
[22] R. Huang, Z. Suo, J.H. Prevost, W.D. Nix, J. Mech. Phys. Solid 50 (2002) 1011.
[23] J. Li, F. Spaepen, T.C. Hufnagel, Philos. Mag. A 82 (2002) 2623.
[24] Z. Bian, G. He, G.L. Chen, Scr. Mater. 46 (2002) 1071.
[25] J. Lu, G. Ravichandran, W.L. Johnson, Acta Mater. 51 (2003) 3429.
[26] J. Wright, T.C. Hufnagel, W.D. Nix, J. Appl. Phys. 93 (2003) 1432.
[27] H.J. Leamy, H.S. Chen, T.T. Wang, Metall. Trans. 3 (1972) 699.
[28] C.T. Liu, L. Heatherly, D.S. Easton, C.A. Carmichael, J.H. Schneibel, C.H. Chen, et al., Metall. Mater. Trans. A 29 (1998) 1811.
[29] Z.F. Zhang, G. He, J. Eckert, L. Schultz, Phys. Rev. Lett. 91 (2003) 045505-1.
[30] P.E. Donovan, Mater. Sci. Eng. 98 (1988) 487.
[31] S. Takayama, Scr. Metall. 13 (1979) 463.
[32] C. Fan, A. Inoue, Mater. Trans. JIM 40 (1999) 1376.
[33] A. Inoue, H.M. Kimura, T. Zhang, Metall. Mater. Trans. A 294–296 (2000) 727.
[34] A. Inoue, W. Zhang, T. Zhang, K. Kurosaka, Acta Mater. 49 (2001) 2645.
[35] D.M. Owen, A.J. Rosakis, W.L. Johnson. In: A. Inoue, C.T. Liu, (Eds.), MRS Symp. Proc. 554 (1999) 419.
[36] H.A. Bruck, A.J. Rosakis, W.L. Johnson, J. Mater. Res. 11 (1996) 503.
[37] T.C. Hufnagel, T. Jiao, Y. Li, L.Q. Xing, K.T. Ramesh, J. Mater. Res. 17 (2002) 1441.
[38] R. Maddin, T. Masumoto, Mater. Sci. Eng. 9 (1972) 153.
[39] Y. Kawamura, T. Shibata, A. Inoue, T. Masumoto, Scr. Mater. 37 (1997) 431.
[40] T. Mukai, T.G. Nieh, Y. Kawamura, A. Inoue, K. Higashi, Scr. Mater. 46 (2002) 43.
[41] C.A. Schuh, T.G. Neih, Acta Mater. 51 (2003) 5187.
[42] C.A. Schuh, A.S. Argon, T.G. Neih, J. Wadsworth, Philos. Mag. A 83 (2003) 2585.
[43] C.A. Schuh, T.G. Neih, J. Mater. Res. 19 (2004) 46.
[44] A.L. Greer, A. Castellero, S.V. Madge, I.T. Walker, J.R. Wilde, Mater. Sci. Eng. A 375–377 (2004) 1182.
[45] T.G. Nieh, C.A. Schuh, J. Wadsworth, Y. Li, Intermetallics 10 (2002) 1177.
[46] W.H. Jiang, M. Atzmon, J. Mater. Res. 3 (2003) 755.
[47] L.H. Dai, L.F. Liu, M. Yan, B.C. Wei, J. Eckert, Chin. Phys. Lett. 21 (8) (2004) 1593.
[48] L.W. Meyer, S. Manwaring, in: Metallurgical Applications of Shock-wave and High-strain-rate Phenomena, Marcel Dekker, New York, 1986.
[49] M.A. Meyers, V.F. Nesterenko, J.C. LaSalvia, Q. Xue, Mater. Sci. Eng. A 317 (2001) 204.
[50] M.A. Meyers, Y.B. Xu, Q. Xue, M.T. Perez-Prado, T.R. McNelley, Acta Mater. 51 (2003) 1307.
[51] D.M. Chen, J.F. Sun, J. Shen, D.W. Xing, L.F. Liang, Mater. Sci. Tech. 12 (6) (2004) 662 (in Chinese).
[52] T. Mukai, T.G. Nieh, Y. Kawamura, A. Inoue, K. Higashi, Intermetallics 10 (2002) 1071.
[53] J. Fineberg, S.P. Gross, M. Marder, H.L. Swinney, Phys. Rev. Lett. 67 (1991) 457.
[54] M.H. Cohen, D. Turnbull, J. Chem. Phys. 31 (5) (1959) 1164.
[55] D. Turnbull, M.H. Cohen, J. Chem. Phys. 34 (1) (1961) 120.
[56] T. Benameur, K. Hajlaoui, A.R. Yavari, A. Inoue, Mater. Trans. 43 (2002) 2617.
[57] M. Reiner, Phys. Today (1964) 62.
[58] Y.L. Bai, M.F. Xia, H.Y. Wang, F.J. Ke, Particuology 1 (1) (2003) 7.